Activity-Based Bioluminescent Logic-Gate Probe Reveals Crosstalk Between the Inflammatory Tumor Microenvironment and ALDH1A1 in Cancer Cells

Chelsea B. Swartchick, Musa Dirak, Lily C. F. Wenger, Rodrigo Tapia Hernandez, Michael C. Lee, and Jefferson Chan*

Read Online

ACCESS | Metrics & More | Article Recommendations | Supporting Information

ABSTRACT: Cancer cells with high expression of aldehyde dehydrogenase 1A1 (ALDH1A1) are more resistant to chemotherapy, contribute to tumor progression, and are associated with poor clinical outcomes. ALDH1A1 plays a critical role in protecting cells from reactive aldehydes and, in the case of stem cells, regulates their differentiation through the retinoic acid signaling pathway. Despite the importance of this enzyme, methods to study ALDH1A1 high-expressing cancer cells in vivo remain limited.

In this work, we developed AlDeLuc, the first logic-gated bioluminescence probe designed to selectively evaluate ALDH1A1 activity in tumor cells. The probe is sequentially activated by acidic intracellular compartments (i.e., endosomes) and ALDH1A1, ensuring precise detection of ALDH1A1 high-expressing cells and minimizing off-target detection of non-ALDH1A1 cells. Beyond demonstrating efficacy in multiple cancer cell lines and a murine model of breast cancer, we employed AlDeLuc to investigate how the population of ALDH1A1 high-expressing cells is influenced by the inflammatory status of a tumor in the context of a high-fat diet. These findings establish a molecular link between obesity, inflammation, and tumor progression.

KEYWORDS: aldehyde dehydrogenase 1A1, inflammation, cancer cells, bioluminescence

INTRODUCTION

Cancer cells with high expression of aldehyde dehydrogenase 1A1 (ALDH1A1) are known for their resistance to chemotherapy, their contribution to tumor progression, and their association with poor clinical outcomes.[1,2] ALDH1A1, part of a superfamily of 19 enzymes, catalyzes the oxidation of xenobiotic and endogenous aldehydes to their corresponding carboxylates.[3] This enzyme plays a critical role not only in protecting cells from reactive aldehydes but also in regulating differentiation in stem cells through the retinoic acid signaling pathway.[4] For example, cancer stem cells (CSCs), a small subset of cells within tumors, often overexpress ALDH1A1. This upregulation is believed to be a driving factor behind their capacity for self-renewal and their ability to repopulate tumors with aggressive, treatment-resistant cancer cells following therapy.[5] ALDH1A1 has thus emerged as a key biomarker in cancer biology, particularly in stemness-related phenotypes. Despite the importance of ALDH1A1, methods for studying ALDH1A1 high-expressing cancer cells in vivo remain limited. Existing tools are challenged by ALDH1A1's intracellular localization, which precludes the use of antibodies for live cell staining or immunohistochemistry.[6] Moreover, commonly used small-molecule fluorescent indicators, such as ALDE-FLUOR, are unsuitable for live animal imaging as a result of its unchanged fluorescence properties before and after activation

by ALDH, leading to off-target detection.[7,8] Additionally, cross-reactivity with other ALDH isoforms further complicates the accurate study of ALDH1A1 activity.[8,9] Although recent advances have produced fluorogenic probes with ALDH1A1 selectivity, issues such as background autofluorescence restrict their utility to cell cultures, excised tissues, or superficial tumor layers.[10,11] Therefore, there remains an unmet need for a reliable method to detect and study ALDH1A1 high-expressing cells within the tumor microenvironment (TME).

Given the goal of developing a tool capable of probing ALDH1A1 activity in vivo, we turned to bioluminescence imaging due to its inherent low background signal. This technique, when combined with activity-based sensing (ABS) probes, has proven effective in detecting rare events and low-abundance cell populations.[12] ABS probes have been engineered to respond to specific analytes, such as nitric oxide, hydrogen peroxide, and redox-active metal ions, by modulating the bioluminescence readout based on chemical
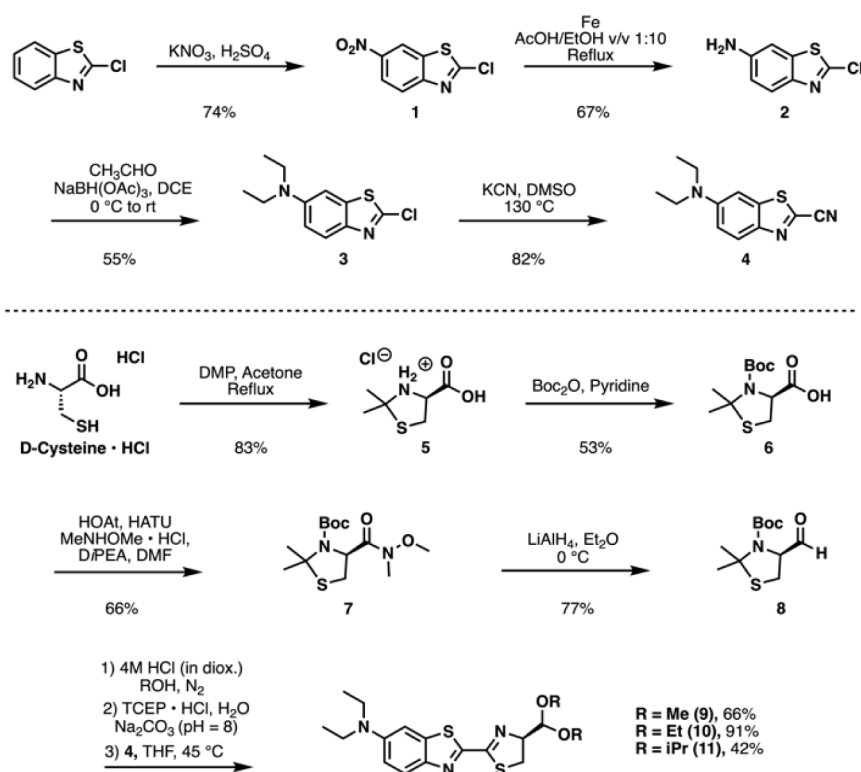
Scheme 1. Schematic Showing the Logic-Gated Activation of AlDeLuc to Yield a Bioluminescence Signal in Response to Sequential Exposure to Acidic Endosomes and ALDH1A1 Activity
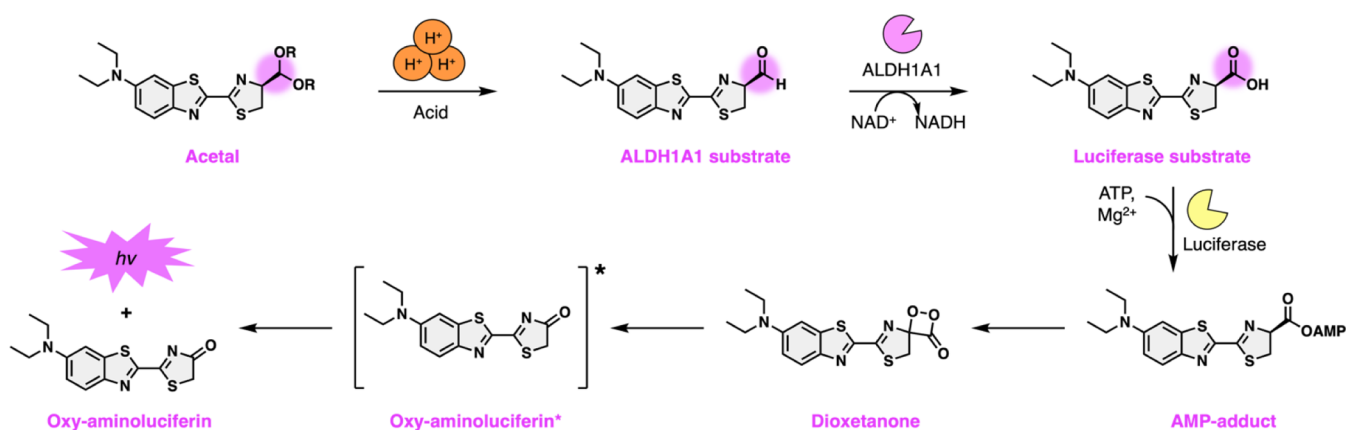

Scheme 2. Synthetic Route to Yield Panel of Logic-Gated Bioluminescent Probes for ALDH1A1 Activity

reactivity.[13−22] For ALDH1A1, several factors, including pH fluxes, NAD+ availability, and substrate concentration, influence enzyme activity and thus need to be considered in probe design.[23] One of the major challenges in detecting ALDH1A1 activity in cancer cells lies in avoiding interference from noncancerous stem cells, which also express this enzyme.[24] A selective detection method is essential to prevent false positives arising from the activation of the probe in normal stem cells before reaching the tumor (Scheme 1).

In this work, we report the rational design of AlDeLuc, a logic-gated bioluminescence probe that selectively evaluates ALDH1A1 activity in cancer cells. AlDeLuc is activated through a sequential "AND" gate mechanism, where the probe first responds to acidic intracellular compartments which are commonly found in cancer cells, followed by ALDH1A1 activity.[25,26] Normal stem cells, which do not exhibit the same

acidic intracellular environment, do not trigger the probe, ensuring specific detection of ALDH1A1 activity in cancer cells. Our probe demonstrates high selectivity against other ALDH isoforms and reactive biological species, producing a strong signal only in the presence of both biomarkers. Furthermore, we validated the probe in multiple cancer cell lines and in vivo using a murine model of breast cancer. Finally, we explored the potential role of inflammation in modulating the population of ALDH1A1 high-expressing cells by conducting experiments in cytokine-activated cultured cancer cells and in chronically obese animals fed a high-fat diet. Our findings suggest a molecular link between inflammation, obesity, and the stemness profile of cancer cells, as modulated by ALDH1A1 activity, offering new insights into the relationship between the TME and cancer progression.
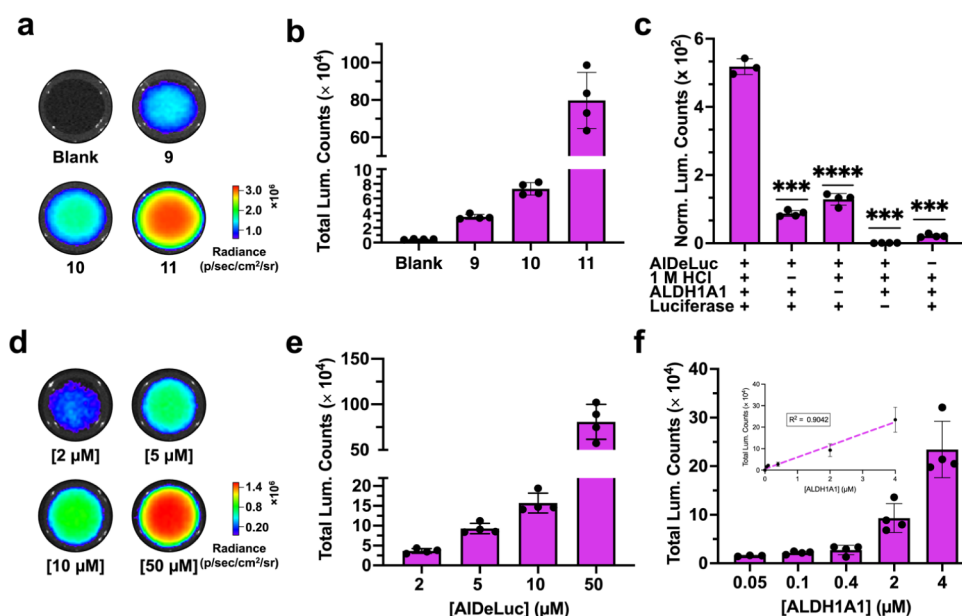
Figure 1. a) Bioluminescent images of compounds 9, 10, and 11 (100 μM) after 60 min incubation with 1 M HCl, treatment with ALDH1A1 (0.4 μM), and luciferase. b) Quantified data from a. c) In vitro assay demonstrating all components: AlDeLuc, acid-hydrolysis, ALDH1A1, and luciferase, must be present to generate bioluminescence. d) Bioluminescent images demonstrating signal intensity is dependent on the concentration of AlDeLuc present. e) Quantified data from d. f) Bioluminescent signal after AlDeLuc (5 μM) is incubated with various amounts of ALDH1A1 and the linear relationship between luminescence and ALDH1A1 concentration. Luciferase concentration was held constant at 0.02 mg/mL for all experiments. Statistical analysis was performed using two-tailed Student's t test with Welch's correction (a = 0.05), ***$r < 0.001$, ****$r < 0.0001$.

RESULTS AND DISCUSSION

Design and Synthesis of Logic-Gate Probes

To achieve the requisite properties to detect ALDH1A1 activity within cancer cells, three critical design criteria were prioritized. First, besides ALDH1A1, the body expresses 18 other ALDH isoforms that are each capable of oxidizing various aldehyde substrates to their corresponding carboxylic acid products. Based on our previous work in developing various isoform-selective ABS probes,[10,11,27−29] we discovered that in the case of ALDH1A1, reactivity is favored when the aldehyde moiety is attached to cyclic structures such as a phenyl ring due to their geometric fit within the enzyme binding pocket. Therefore, we hypothesized that substituting the carboxylic acid group of firefly luciferin at the 4,5-dihydrothiazole core with an aldehyde would impart comparable selectivity for the ALDH1A1 isoform. Moreover, because the carboxylic acid is essential for luciferase recognition, binding and turnover,[30] the aldehyde would therefore represent an inert trigger in the absence of ALDH1A1. Second, anticipating that ALDH1A1 activity may occur at sites other than at the tumor (e.g., mesenchymal stem cells (MSCs)), we further converted the aldehyde into an acid-responsive acetal group. This design can potentially exploit the acidic TME,[25] but more likely acidic endosomes[26] that are abundant in cancer cells to mediate site-specific probe activation. Lastly, we strategically replaced the pH-sensitive phenol with a pH-insensitive N,N-diethyl aniline to ensure that the bioluminescence signal will remain constant. With these criteria in mind, we devised a modular synthetic route to access the requisite building blocks for the proposed logic-gated probe for ALDH1A1.

First, 2-chlorobenzothiazole was subjected to standard electrophilic aromatic substitution conditions to yield the mononitrated intermediate 1 in 74% yield (Scheme 2). A Beauchamp reduction was then employed to convert the aromatic nitro group to the corresponding aniline 2 in 67%, which allowed for subsequent installation of ethyl groups via reductive amination to afford the N,N-diethylamino intermediate 3 in 55% yield. Treatment of 3 with potassium cyanide afforded the cyano-benzothiazole 4 via SNAr chemistry in 82% yield. In parallel, D-cysteine hydrochloride was reacted with dimethoxypropane in acetone to furnish the 2,2-dimethylthiazolidine intermediate 5 in 83% yield. The secondary amine was Boc-protected to yield 6, and its carboxylic acid group was transformed to the Weinreb-amide intermediate 7 in 35% over two-steps. Lithium aluminum hydride was then employed to access the aldehyde 8 in 77% yield. With this in hand, we attempted to mask the aldehyde as an acetal, which was followed by deprotection of the Boc-group and 2,2-dimethylthiazolidine core. This sequence was initially unsuccessful as the major products formed were the imidate and the thioamide (Figure S1). After extensive screening, we found its formation could be suppressed by rigorously degassing the alcohol solvent used for the acetalization step, as well as performing deprotection of the 2,2-dimethylthiazolidine under an inert nitrogen atmosphere. After 2 days, the solvent could then be exchanged for degassed THF containing 4 to give the desired acetal product(s). By varying the alcohol solvent (i.e., methanol, ethanol, and isopropanol), we were able to access acetals 9, 10, or 11.

In Vitro Evaluation of Acetal Trigger Stability

After obtaining 9, 10 and 11, our goal was to first identify the most acid-resistant acetal to ensure stability while in circulation. The aldehyde intermediate exists in an equilibrium with its hydrate form (Figure S2), complicating detection and quantification using HPLC-MS. As such, we utilized bioluminescence to investigate hydrolytic stability. Each molecule

was incubated in 1 M HCl for one hour, neutralized and sequentially treated with ALDH1A1 and luciferase prior to imaging (λ_{em} = 605 nm at pH 7.4 and temp. = 37 °C). Compound 9 was deemed the most acid resistant as treatment yielded the lowest bioluminescence (Figures S3, 1a,b). This finding is consistent with reported acetal stability trends.[31] To further these results, we show that AlDeLuc can be activated at pH values ranging from 4.5 to 6.0, consistent with the endosomal compartment (Figure S4a). In contrast, no bioluminescence was observed when treated with 1 M NaCl or 1 M NaOH, indicating no acetal unmasking at neutral or alkaline pH values (Figure S4b). Similarly, incubation in neutral PBS or serum-containing media yielded identical results (Figure S5).

We subsequently examined potential off-target activation by glucosidases (e.g., beta-galactosidase (β-Gal)) owing to their ability to hydrolyze acetals to hemiacetals, which in the case of 9 would further decompose to yield an aldehyde substrate. Even in the presence of 1 unit of β-Gal (1 unit = 1 μmol substrate converted per min at pH 7.3 at 37 °C) which was confirmed for activity, the acetal remained completely stable (Figures S6 and S7). Additionally, we treated 9 with rat liver microsomes at various concentrations to account for possible CYP450 activity (e.g., CYP3A4) that has been reported to cleave acetals.[32] Across a range of concentrations from 0.25 to as high as 5.0 ng/mL, negligible bioluminescence was observed (Figure S8). We obtained similar results when AlDeLuc was directly treated with commercial supersomes enriched with CYP3A4. Compared to ALDH1A1 the signal enhancement was negligible (Figure S9). Collectively, these results indicate that the dimethyl acetal satisfies our logic-gate design criteria and thus, 9 will herein be referred to as AlDeLuc.

Mechanism of AlDeLuc Logic-Gate Activation

Next, to examine the mode of AlDeLuc activation, we performed assays where exposure to acidic conditions and ALDH1A1 were investigated separately (Figure 1c). Compared to when both conditions were applied, the signal of AlDeLuc upon treatment with luciferase was significantly attenuated, which is consistent with the envisioned logic-gate mechanism. Likewise, when either AlDeLuc or luciferase was excluded, the bioluminescent signal was also negligible. Next, we varied the concentration of AlDeLuc from 2 to 50 μM and observed a concentration-dependent increase in signal intensity (Figure 1d,e). Likewise, when the concentration of AlDeLuc was held constant and the amount of ALDH1A1 was varied (from 0 to 4 μM), we noted that the wells with the highest ALDH1A1 concentration showed the most intense signal (Figure 1f).

Although these results collectively demonstrate that AlDeLuc is a competent substrate for ALDH1A1 after acetal removal, it is critical to examine potential cross-reactivity with other common ALDH isoforms, as some may also be elevated in CSCs.[33] After expressing and purifying ALDH1A2, ALDH1A3, ALDH2, ALDH3A1, ALDH4A1, and ALDH5A1, we measured each enzyme's activity using their preferred aldehyde substrates. Afterward, AlDeLuc was preactivated with HCl, neutralized, and incubated with the same enzyme unit for each isoform (1 unit = 0.5 nmol/min). Only treatment with ALDH1A1 and luciferase generated significant bioluminescence (Figure 2a). To account for scenarios where a non-ALDH1A1 isoform may be present at a higher concentration relative to ALDH1A1, we increased the enzyme unit to 5 units
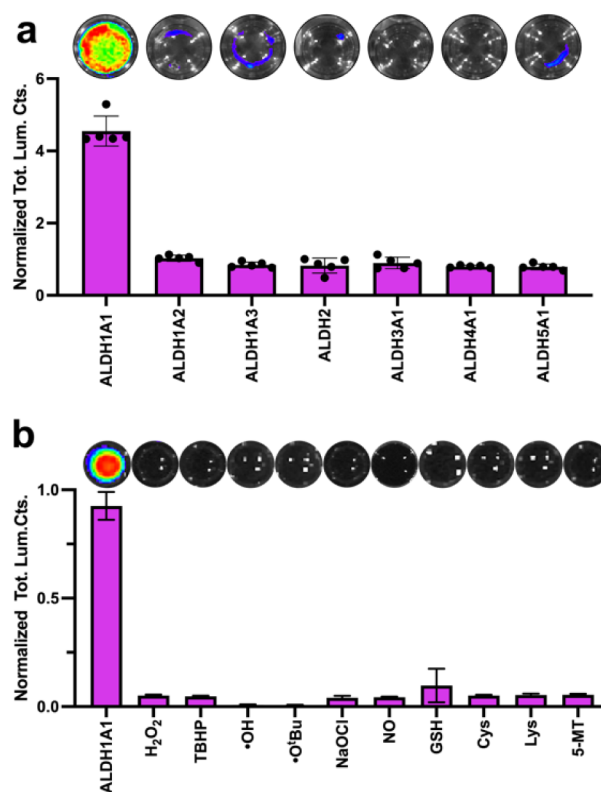
Figure 2. a) Normalized bioluminescence of AlDeLuc (2 μM) upon incubation with each ALDH isoform (1 unit = 0.5 nmol/min) after 60 min at room temperature (n = 5). b) Response of AlDeLuc (50 μM) after incubation with various reactive oxygen and nitrogen species, biological thiols, and amines at concentrations of 100 μM. Cys and GSH were tested at 1 mM. ALDH1A1 activation is provided for reference. Luciferase (0.005 mg/mL) was added to initiate bioluminescence production. (n = 3).

while holding ALDH1A1 at 1 unit. Consistent with the equal-unit experiment, minimal off-target activation was noted (Figure S10). We corroborated these results by monitoring the absorbance change at 340 nm, which is indicative of NADH production during aldehyde oxidation (Figure S11). Beyond testing common ALDH isoforms, we assessed the potential oxidation of the aldehyde to the corresponding carboxylic acid due to high levels of reactive oxygen species in cancer cells. No interference was found upon treatment of the aldehyde form of AlDeLuc with peroxides (e.g., H_2O_2, tert-Butyl hydroperoxide), radicals (e.g., $\cdot$OH, $\cdot$OtBu), or hypochlorite (Figure 2b). Lastly, we examined whether the presence of glutathione and amino acids such as lysine and cysteine would attenuate ALDH1A1-catalyzed oxidation due to their ability to form Schiff bases[34] or thiazolidines,[35] respectively. Additionally, we tested 5-methoxytryptamine, which is known to react with aldehydes via Pictet-Spengler chemistry.[36] The presence of these analytes did not attenuate the bioluminescence compared to control reactions where they were excluded.

Evaluation of AlDeLuc in Bone Marrow Mesenchymal Stem Cells and A549 Human Lung Cancer Cells

Our next objective was to evaluate the performance of AlDeLuc in live cells to assess uptake, activation, and possible interference from components of the complex cellular milieu. For this purpose, we obtained mesenchymal stem cells (MSCs) (CD34+, ALDH1A1+) from a commercial vendor

(ATCC).[37,38] We followed recommended culturing procedures to obtain ~2.5 × 10^5 cells that were undifferentiated and viable (Supporting Information). MSCs were selected as the noncancerous counterpart because they overexpress ALDH1A1 and in comparison to cancer cells, are known to exhibit a more neutral pH within their intracellular compartments.[39−41]

Testing commenced by incubating MSCs with AlDeLuc (20 μM). After one hour, the cells were lysed, treated with luciferase, and imaged. Notably, we devised this procedure where luciferase was supplemented because the MSCs we obtained are genetically unmodified. Moreover, we wanted to allow for any oxidized N,N-diethyl luciferin substrate to accumulate for the highest possible signal. The bioluminescence of cells treated with AlDeLuc was indistinguishable from blank controls indicating that probe activation had not occurred in the MSCs tested (Figure 3a).
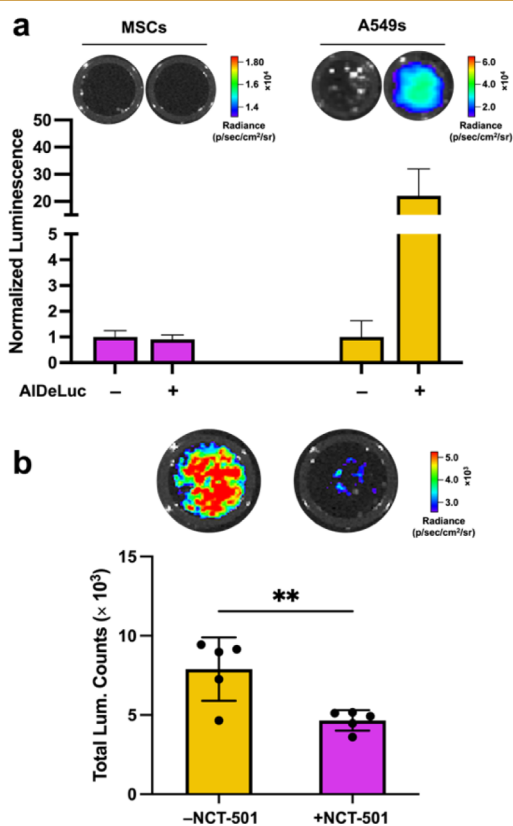
Figure 3. a) Representative images of MSC or A549 cell lysates after treatment with AlDeLuc for 1 h, then treatment with luciferase. b) Representative bioluminescent images of A549 cell lysates after cotreatment with NCT-501 (ALDH1A1-specific inhibitor) (40 μM) and AlDeLuc (20 μM) for 1 h followed by addition of luciferase. Luciferase concentration held constant at 0.05 mg/mL and n = 4 for all experiments. Statistical analysis was performed using two-tailed Student's t test with Welch's correction (α=0.05), **ρ < 0.01.

After evaluating AlDeLuc in MSCs, we further chose to use A549 human lung carcinoma cells to evaluate its performance in cancer cells. A549 cells are ideal for this application owing to their higher expression levels of ALDH1A1 compared to other cell types, with concentrations typically in the nanomolar (nM) range.[42,43] When we repeated the experiment using only half the number of A549 cells relative to the number of MSCs (~1.25 × 10^5 cells), we observed that the light emission was

22.1-fold higher than the vehicle controls (Figure 3a). By increasing the number of A549 cells, the bioluminescence intensity increased in a cell number-dependent manner (e.g., 56-fold for 3.6 × 10^6 A549 cells) (Figure S12). We attribute the stark difference of AlDeLuc behavior in MSCs and A549 cells due to the presence of our logic-gate design featuring the acetal trigger. Next, to confirm activation of AlDeLuc was due to ALDH1A1 activity, we utilized NCT-501, a selective inhibitor of human ALDH1A1.[44] We observed a marked reduction of 1.7-fold in bioluminescence with respect to vehicle controls (Figure 3b). Comparable results from A549 cells were obtained when this was repeated using luciferase-expressing A549 cells (Figure S13). This critical finding demonstrates that AlDeLuc is an effective reporter of ALDH1A1 activity in a cellular context.

Assessment of AlDeLuc in 4T1 Murine Breast Cancer Cells

In addition to our investigation in a human lung cancer cell line, we performed additional experiments using cultured 4T1 murine mammary carcinoma cells. Recently, we demonstrated that a chronic inflammatory response, driven by diet-induced nitric oxide (NO) production, increases tumor aggressiveness, growth, and potentially stemness characteristics in 4T1 tumors.[22] Given the pivotal role of ALDH1A1 activity in these processes, we posited that altering NO levels may affect the activity of this key enzyme as NO has been shown in other systems such as rat livers exposed to ethanol to inhibit ALDHs via S-nitrosylation of the active site cysteine residue.[45] With the AlDeLuc technology in hand, we were in position to determine whether ALDH1A1 activity in living systems is indeed altered in the presence of NO.

First, we showed via MTT analysis that like with A549 cells, AlDeLuc was also nontoxic up to the highest concentration tested in 4T1 cells (100 μM) (Figure S14). Next, we treated the 4T1 cells with AlDeLuc to measure ALDH1A1 activity. For this assay, we used nonluciferase expressing 4T1 cells to precisely control the timing of the bioluminescence signal generation (via addition of exogenous luciferase) to facilitate accurate measurements. Consistent with previous reports documenting high ALDH1A1 expression levels in this cell line,[46] we observed a significant 42-fold increase in bioluminescence as compared to blank controls (Figure 4a). To investigate whether the results from these studies were attributable to ALDH1A1 activity, we again employed NCT-501 to selectively inhibit this isoform. Relative to uninhibited cells, application of the inhibitor resulted in a diminished bioluminescent signal of approximately 2.2-fold (Figure 4b). It is important to acknowledge that the murine ALDH1A1 isoenzyme exhibits distinct structural and enzymatic properties compared to its human counterpart which may potentially influence the potency of inhibitors such as NCT-501. While NCT-501 demonstrates strong selectivity for human ALDH1A1, its potency against murine ALDH1A1 remains uncharacterized, which may partially account for the attenuated inhibition observed in 4T1 cells relative to A549 cells. In addition, we confirmed our results using diethylaminobenzaldehyde (DEAB), a competitive and reversible ALDH inhibitor. DEAB was also tested owing to its established use in cellulo and in vivo to inhibit murine ALDH1A1 found in 4T1 cells (Figure S15). Despite its broader inhibition profile, DEAB produced consistent results, further validating our findings.[47] These results collectively affirm the efficacy of AlDeLuc as a sensitive and reliable reporter of ALDH1A1 activity in 4T1
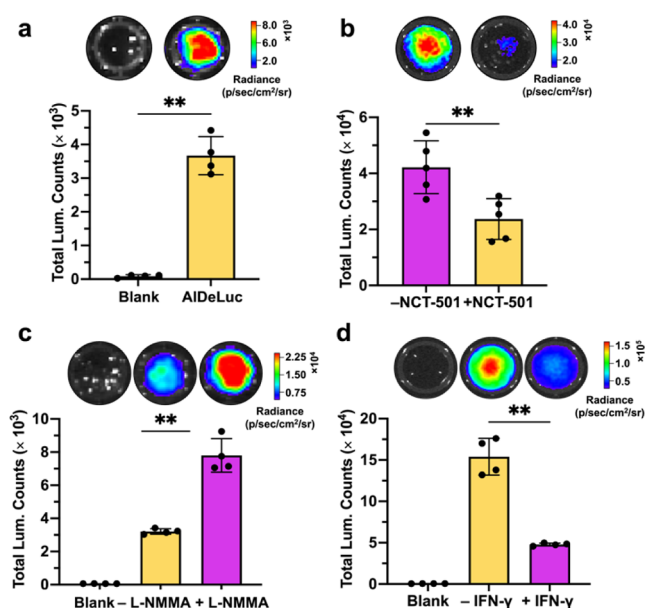
Figure 4. a) 4T1 cell lysates incubated with AlDeLuc (100 μM) for 60 min then administered luciferase. $n = 4$ b) Representative bioluminescence images of 4T1 lysates after cells were cotreated with NCT-501 (40 μM) (or vehicle) and AlDeLuc (20 μM) for 60 min then administered luciferase. $n = 5$ c) Representative images of 4T1 cells pretreated with L-NMMA (1 mM) or vehicle, followed by AlDeLuc (50 μM) and subsequent addition of luciferase to cell lysates. $n = 4$ d) Representative luminescent images of 4T1 cell lysates pretreated with IFN-γ (26.8 ng/mL) or vehicle for 12 h, then administered AlDeLuc (50 μM) and luciferase, $n = 4$. Luciferase concentration held constant at 0.05 mg/mL. Blank = protease buffer. Statistical analysis was performed using two-tailed Student's t test with Welch's correction (a = 0.05), **$r < 0.01$.

murine cells, setting the stage for its use in exploring potential crosstalk with the inflammatory response.

As mentioned, we previously discovered that treatment of 4T1 cells with DEA NONOate (50 μM), an NO donor, or L-NMMA (1 mM), a nonspecific inhibitor of NOS, were effective at increasing or decreasing intracellular levels of NO, respectively (Figure S16).[22] In this study, when AlDeLuc was applied to L-NMMA-treated cells the corresponding bioluminescence was found to be 2.4-fold higher compared to vehicle-treated cells. This difference in signal indicates that attenuating NO levels has an effect of elevating ALDH1A1 activity (Figure 4c). Based on this finding, we posited that stimulation of NO production should therefore have the opposite effect. To investigate this hypothesis, we first delivered NO exogenously using DETA NONOate, a NO donor exhibiting a long half-life ($t_{1/2} = 20$ h) to mimic chronic release of NO in the TME. When AlDeLuc was subsequently employed to image ALDH1A1 activity, we found the bioluminescence was decreased by 1.3-fold (Figure S17). Next we exposed 4T1 cells to either lipopolysaccharides (LPS) or interferon gamma (IFN-γ) which have both been shown to stimulate NO production via inducible nitric oxide synthase (iNOS).[47] Similar to what we observed for NO supplementation, the bioluminescence signals when treated with LPS or IFN-γ were attenuated 1.2-fold (Figure S18) and 3.2-fold (Figure 4d) relative to vehicle-treated control cells, respectively. While these results underscore an interaction between NO levels and ALDH1A1 activity, it is crucial to acknowledge that cellular models cannot fully recapitulate the TME.

Additionally, it is important to recognize that the timing and dosage of NO production (acute versus chronic) can have vastly different effects on cancer cell properties. Furthermore, the hydrolysis of the AlDeLuc acetal produces methanol, which is metabolized to formaldehyde. Formaldehyde reacts with glutathione, forming S-nitrosoglutathione (GSNO), which is metabolized by glutathione-dependent formaldehyde dehydrogenase (GSNOR). This reaction generates NADH and reduced glutathione, potentially altering NO flux. Such interactions could introduce metabolic crosstalk, influencing NO levels and ALDH1A1 activity in complex and context-dependent ways.

In Vivo Evaluation of AlDeLuc in 4T1 Murine Breast Tumors

Following these pivotal cellular experiments, we next evaluated AlDeLuc within an in vivo setting (Figure S19). To establish whether AlDeLuc exhibits a favorable safety profile, we administered AlDeLuc systemically at doses of 0.55 mg/kg. After four hours, the animals were sacrificed and their vital organs including the spleen, kidneys, lungs, heart, and liver were excised for hematoxylin and eosin (H&E) staining (Figure 5a). Compared to control animals that received a vehicle, the stains were indistinguishable, demonstrating AlDeLuc is biocompatible (Figure 5b). Subsequently, BALB/c mice (~5 weeks old) were inoculated on their flanks with 4T1-Luc cells (1×10^5) to establish heterotopic breast tumors. After approximately 3 weeks, the average tumor volume reached ~250 mm^3. AlDeLuc was then administered systemically, and the bioluminescence output was monitored for 24 h by delineating regions of interest (ROIs) around each tumor and summing the total luminescent counts for each mouse. Of note, no bioluminescence was observed outside of these ROIs. AlDeLuc activation was rapid, with a detectable signal from the first scan that plateaued after 40 min and was absent at the 24-h mark, indicating complete clearance (Figure S20). This rapid clearance was crucial as it permitted subsequent experiments to confirm ALDH1A1 involvement with the same subjects, thereby minimizing variability as opposed to using a separate cohort of tumor-bearing animals. Specifically, 2 days later, mice were cotreated with DEAB and AlDeLuc via retroorbital injection. A significant attenuation of total luminescent counts was observed in animals cotreated with DEAB ($0.78 \pm 0.28 \times 10^4$) compared to those administered AlDeLuc alone ($2.18 \pm 0.60 \times 10^4$) (Figure 5c,d). This represents a 2.8-fold difference and demonstrates AlDeLuc's successful hydrolysis in the acidic endosomes and its capability to detect ALDH1A1 activity in vivo.

Diet-Induced Inflammation Modulates ALDH1A1 Activity in a Murine Model of Breast Cancer

Finally, to examine how NO influences ALDH1A1 activity in vivo we placed BALB/c mice (female, 5−7 weeks old) on a high-fat diet for 40 weeks to induce an inflammatory response through elevated NO production. This period consisted of a ~20-week priming period prior to inoculation of the animals with 4T1-Luc cells at the mammary fat pad. At this point, the mice were randomized into two groups. The treatment group was administered L-NMMA (50 mg/kg), whereas the control group received water via oral gavage for 20 days. The day after the final treatment, mice from both conditions were treated systemically with AlDeLuc, and the bioluminescence was monitored (Figure 5e). The group administered the NOS inhibitor had a 5.9-fold enhancement in total luminescent
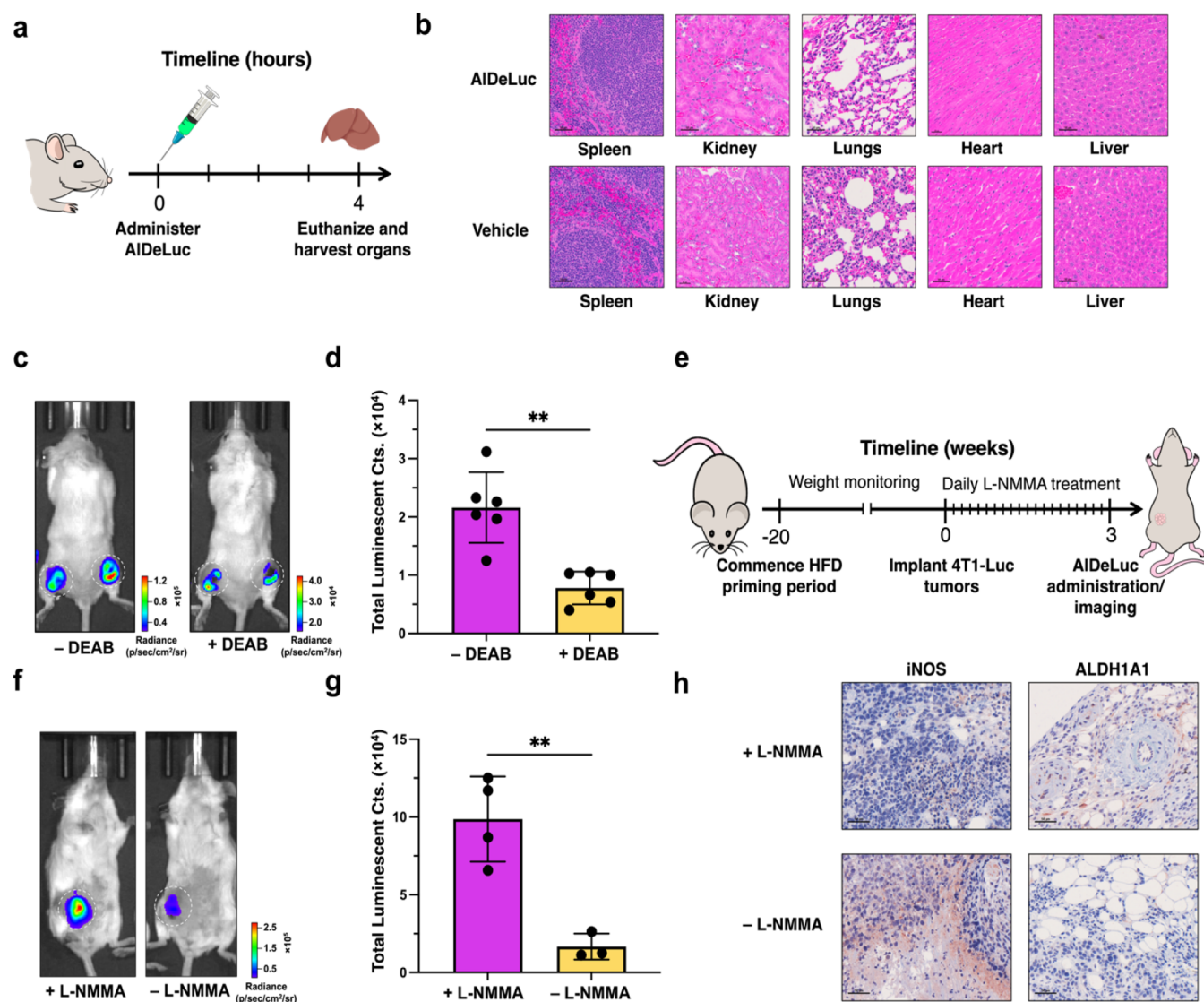
Figure 5. a) Timeline of the AlDeLuc systemic toxicity investigation. b) Hematoxylin and eosin stains of the major organs from mice administered either AlDeLuc or vehicle to evaluate the biocompatibility of our probe. Scale bar represents 50 μm. c) Representative bioluminescent images of BALB/c mice bearing 4T1-Luc tumors acquired 40 min after systemic administration of AlDeLuc (left) or mixture of AlDeLuc and DEAB solution (right). d) Quantified data from c. e) Timeline of high-fat diet (HFD) induced-inflammatory murine model generated to explore the influence of NO on ALDH1A1 activity using AlDeLuc. f) Representative bioluminescent images of BALB/c mice bearing orthotopic mammary 4T1-Luc tumors after a 20-week HFD priming period that were either administered L-NMMA (50 mg/kg) (left) or water (right) via oral gavage daily for 3 weeks and were retro-orbitally administered AlDeLuc (0.55 mg/kg). Images were collected 40 min after injection. g) Quantified data from f. h) Immunohistochemical stains of 4T1-Luc tumors with iNOS or ALDH1A1 antibodies from mice treated with L-NMMA (+ L-NMMA) or vehicle ($-$ L-NMMA). Statistical analysis was performed using two-tailed Student's t test with Welch's correction (α=0.05), **$\rho < 0.01$. Scale bar represents 50 μm.

counts as compared to the control group ($9.9 \pm 2.7 \times 10^4$ and $1.7 \pm 0.8 \times 10^4$ respectively) (Figure 5f,g). At the completion of the diet study, animals were sacrificed, and their tumors were excised for further immunohistochemical analysis. Specifically, we determined that iNOS expression in tumors treated with L-NMMA was reduced. Not only does this result indicate, iNOS inhibition was successful but that the total amount of protein had also decreased. On the other hand, we observed the opposite trend for ALDH1A1 expression (Figure 5h). Collectively, our results provide compelling evidence that an excessive inflammatory TME modulates ALDH1A1 activity, which in term may alter the aggressiveness of cancer cells.

■ CONCLUSION

Understanding cancer progression requires deep insight into the critical role of ALDH1A1-high expressing cells their dynamic interplay with the TME. In this work, we have developed a bioluminescent logic-gated probe specifically for in vivo detection of such cancer cells. Bioluminescence was chosen over other imaging modalities for its low background and high sensitivity, which are particularly advantageous for detecting ALDH1A1-high cells which may only account for a fraction of the tumor mass.[48] To prevent false positives due to ALDH1A1 activity at distal sites, such as within healthy tissues, we engineered a new ABS trigger that requires a two-step activation mechanism: first by the acidic endosomes and subsequently by ALDH1A1, to produce the active amino

luciferin substrate. While several bioluminescent probes that employ dual activation exist,[21,49−51] AlDeLuc represents the first probe of its kind that has been optimized to consider the activity of both targets, specifically fine-tuning of the acid-responsive group for stability in circulation and robust unmasking in acidic endosomes, as well as the aldehyde substrate for exceptional ALDH1A1 isoform selectivity. This feature was showcased in pivotal cellular experiments where AlDeLuc activation was assessed head-to-head in MSCs (normal stem cells) and A549 cancer cells. Existing probes lack this key features and therefore are only suitable for in vitro testing under stringent conditions.[52] Of note, we also demonstrated that the acetal moiety of AlDeLuc did not exhibit cross reactivity with CYP450s such as CYP3A4 as was reported for similar chemical structures.[32]

In our cellular studies, AlDeLuc revealed a previously uncharted interaction between ALDH1A1 activity and NO modulators like IFN-γ and L-NMMA, prompting us to explore this dynamic in vivo with an intact TME. As previously reported, we fed mice a high-fat diet to induce obesity, leading to visceral fat accumulation (Figure S21). Fat deposits in organs such as the liver and mammary fat pads are known to promote a chronic inflammatory state through NO over-production.[53] Ensuing AlDeLuc imaging uncovered a novel link between the TME's inflammatory milieu and ALDH1A1 activity. This critical insight suggests that modulating NO levels could be a strategic approach to altering the aggressiveness of cancer cells via ALDH1A1 and this research is actively being pursued in our laboratory.

In closing, detecting the crosstalk between NO and ALDH1A1 would not have been feasible without AlDeLuc. However, it is important to note that this technology requires the use of luciferase-expressing cells, limiting its application to preclinical models. Despite this, we anticipate that the AlDeLuc technology will prove invaluable in monitoring ALDH1A1-high cells such as aggressive cancer stem cell populations during preclinical evaluation of chemotherapeutic interventions or assessing the impact of ALDH1A1-targeted treatments.

■ METHODS

Synthesis

Chloro-6-nitrobenzo[d]thiazole (1). H_2SO_4 (51.2 mL) was cooled to 0 °C in an ice-bath. 2-Chlorobenzo[d]thiazole (6 mL, 45.06 mmol, 1 equiv) was then added dropwise to the reaction. While maintaining the temperature at 0 °C, KNO_3 (5.01 g, 49.57 mmol, 1.1 equiv) was added portion-wise over 30 min. After stirring for an additional 30 min, the reaction mixture was warmed to room temperature and stirred overnight. The reaction was quenched via pouring over ice. The solid was then filtered, washed with ice-cold deionized water, and recrystallized in ethanol to give **1** as light-yellow crystals in 74% yield (7.32 g, 33.34 mmol). ^{1}H NMR (500 MHz, CDCl$_3$) δ 8.68 (d, J = 2.2 Hz, 1H), 8.31 (dd, J = 9.0, 2.3 Hz, 1H), 8.01 (d, J = 8.9 Hz, 1H). ^{13}C NMR (126 MHz, CDCl$_3$) δ 158.81, 154.78, 145.44, 136.47, 123.37, 122.27, 117.71.

2-Chloro[d]thiazole-6-amine (2). Iron powder (4.29 g, 76.82 mmol, 4 equiv) was added to a solution of **1** (4.12 g, 19.21 mmol, 1 equiv) in 1:10 v/v acetic acid:ethanol (0.1 M). After stirring at reflux for two hours, the reaction mixture was cooled to room temperature, diluted with ethanol, and filtered over Celite. After the volume of the filtrate was reduced to ~50% under reduced pressure, the remaining liquid was neutralized and extracted using ethyl acetate (×3). The combined organic layers were washed with brine, dried over Na_2SO_4, and concentrated to dryness. The solid residue was purified via recrystallization in ethanol to afford **2** as light purple crystals in 67% yield (2.37 g, 12.86 mmol). ^{1}H NMR (500 MHz, CDCl$_3$) δ 7.70 (d, J = 8.7 Hz, 1H), 6.99 (d, J = 2.3 Hz, 1H), 3.86 (s, 2H). ^{13}C NMR (126 MHz, CDCl$_3$) δ 148.47, 144.94, 144.13, 137.83, 123.39, 115.70, 105.16.

2-Chloro-N,N-diethylbenzo[d]thiazole-6-amine (3). To a solution of **2** (1.33 g, 7.19 mmol, 1 equiv) in dichloroethane (65.40 mL, 0.11 M), acetaldehyde (2.43 mL, 43.16 mmol, 6 equiv) was added. Immediately after addition, sodium triacetoxyborohydride (3.81 g, 17.98 mmol, 2.5 equiv) was added and stirred at room temperature for two hours. The reaction was quenched with methanol and the solvent was concentrated. The residue was redissolved in ethyl acetate, washed with water (×2), dried over sodium sulfate, and concentrated. The crude was then purified via silica gel column chromatography (eluent: 3:97 v/v EtOAc:Hexanes) to afford **3** as a brown oil in 55% yield (0.9515 g, 3.95 mmol). ^{1}H NMR (500 MHz, CDCl$_3$) δ 7.71 (d, J = 9.1 Hz, 1H), 6.90 (d, J = 2.6 Hz, 1H), 6.84 (dd, J = 9.1, 2.6 Hz, 1H), 3.39 (q, J = 7.1 Hz, 5H), 1.19 (t, J = 7.1 Hz, 7H). ^{13}C NMR (126 MHz, CDCl$_3$) δ 146.83, 146.42, 141.81, 138.60, 123.05, 112.65, 101.51, 44.85, 12.52.

6-(Diethylamino)benzo[d]thiazole-2-carbonitrile (4). A round-bottom flask was charged with potassium cyanide (56.85 mg, 0.87 mmol, 2 equiv) and treated with a solution of **3** (105.10 mg, 0.44 mmol, 1 equiv) in DMSO (17 mL, 0.03 M). The reaction was stirred at 130 °C for three hours, cooled to room temperature, and poured onto deionized water (100 mL). The reaction was transferred to a separatory funnel, extracted with EtOAc (×3), dried with Na_2SO_4, and concentrated. The crude residue was purified by silica gel column chromatography (eluent: 7:93 v/v EtOAc:Hexanes) to afford **4** as a yellow solid in 82% yield (0.0828 g, 0.36 mmol). ^{1}H NMR (500 MHz, CDCl$_3$) δ 7.93 (d, J = 9.3 Hz, 1H), 7.00 (dd, J = 9.3, 2.6 Hz, 1H), 6.96 (d, J = 2.6 Hz, 1H), 3.46 (q, J = 7.1 Hz, 5H), 1.23 (t, J = 7.1 Hz, 7H). ^{13}C NMR (126 MHz, CDCl$_3$) δ 148.37, 143.39, 139.14, 128.87, 125.48, 114.46, 114.10, 99.93, 45.01, 12.50.

(S)-4-Carboxy-2,2-dimethylthiazolidin-3-ium chloride (5). To a solution of D-cysteine hydrochloride (21.05 g, 133.56 mmol, 1 equiv) in acetone (530 mL, 0.24 M) was added 2,2-dimethoxypropane (111 mL, 908.56 mmol, 7.16 equiv) and refluxed for 20 h. The reaction was cooled to 50 °C, filtered, and washed with cold acetone. The white crystals were collected to give **6** in 83% yield (21.91 g, 110.85 mmol) and used without further purification. ^{1}H NMR (500 MHz, D$_2$O) δ 4.88 (t, J = 8.1 Hz, 1H), 3.65 (dd, J = 12.2, 8.1 Hz, 1H), 3.52 (dd, J = 12.2, 8.0 Hz, 1H), 1.79 (d, J = 6.9 Hz, 6H). ^{13}C NMR (126 MHz, D$_2$O) δ 169.81, 72.87, 62.15, 31.59, 27.65, 26.61.

(S)-3-(tert-Butoxycarbonyl)-2,2-dimethylthiazolidine-4-carboxylic Acid (6). Di-tert-butyl dicarbonate (11.14 g, 51.04 mmol, 1.1 equiv) was added to a solution of **5** (7.48 g, 46.40 mmol, 1 equiv) in pyridine (45 mL, 1.04 M), flushed with nitrogen, and stirred at room temperature for 2.5 days. The reaction was diluted with toluene, transferred to a separatory funnel, and extracted with ice-cold 2 M sodium hydroxide (×3). The aqueous fraction was washed with toluene (×3), Hexanes (×1), and acidified with aqueous citric acid to pH 3.0. After acidification, the aqueous solution was extracted with dichloromethane (×4). The organic fraction was washed with brine, dried with Na_2SO_4, and concentrated. The resulting crude residue was recrystallized in Hexanes to afford the product as an off-white solid in 53% yield (7.18 g, 29.87 mmol). ^{1}H NMR (500 MHz, CDCl$_3$) δ 11.49−10.76 (m, 1H), 5.11−4.48 (m, 1H), 3.34−3.02 (m, 2H), 1.83−1.66 (m, 6H), 1.40 (d, J = 43.5 Hz, 9H). ^{13}C NMR (126 MHz, CDCl$_3$) δ 177.28, 175.54, 153.74, 151.64, 81.89, 80.97, 71.90, 70.37, 65.95, 65.26, 30.73, 30.32, 29.74, 29.59, 28.69, 28.39, 28.28, 27.95.

tert-Butyl (S)-4-Methoxy(methyl)carbamoyl)-2,2-dimethylthiazolidine-3-carboxylate (7). To a solution of **6** (3.00 g, 11.48 mmol, 1.0 equiv) in DMF (15.3 mL, 0.75 M), was sequentially treated with N,N-diisopropylethylamine (4 mL, 22.96 mmol, 2.0 equiv), hexafluorophosphate azabenzotriazole tetramethyl uronium (HATU) (5.50 g, 14.46 mmol, 1.3 equiv), 1-hydroxy-7-azabenzotriazole (1.77 g, 12.97 mmol, 1.1 equiv), and N,O-dimethylhydroxylamine hydrochloride (2.24 g, 22.96 mmol, 2.0 equiv). The resulting

mixture was stirred at room temperature for 16 h and then diluted with deionized water. The aqueous solution was extracted with EtOAc (×3), washed with 30% citric acid (×2), saturated NaHCO₃ (×2), and brine (×1). It was then dried with Na₂SO₄ and concentrated. The crude residue was purified via silica gel column chromatography (eluent: 2:3 v/v EtOAc:Hexanes) to afford the product as an off-white solid in 66% yield (2.30 g, 7.58 mmol). ^{1}H NMR (500 MHz, CDCl₃) δ 5.11 (d, J = 67.1 Hz, 1H), 3.75 (d, J = 23.1 Hz, 3H), 3.33 (dd, J = 13.5, 7.0 Hz, 1H), 3.21 (s, 3H), 3.01−2.94 (m, 1H), 1.89 (d, J = 13.2 Hz, 6H), 1.45 (d, J = 41.1 Hz, 9H). ^{13}C NMR (126 MHz, CDCl₃) δ 171.61, 171.14, 170.74, 152.88, 151.64, 80.72, 80.30, 72.07, 70.41, 64.77, 63.97, 61.30, 61.19, 60.39, 32.56, 30.87, 30.15, 29.83, 29.32, 28.64, 28.48, 28.42, 27.82, 21.06, 14.20.

tert-Butyl (S)-4-Formyl-2,2-dimethylthiazolidine-3-carboxylate (8). To a solution of **8** (500 mg, 1.64 mmol, 1.0 equiv) in diethyl ether (5.7 mL, 0.29 M) was cooled to 0 °C. In one portion, LiAlH₄ (62.34 mg, 1.64 mmol, 1.0 equiv) was added and the resulting suspension was stirred at the same temperature for 30 min. While on ice, KHSO₄ (30% w/v in deionized water) was added and stirred for an additional 20 min. The solids were filtered and rinsed with diethyl ether. The filtrate was washed with 0.1 M HCl (×1), 10% NaHCO₃ (×1), brine (×2), dried with Na₂SO₄ and concentrated. The crude residue was purified with silica gel column chromatography (eluent: 1:4 v/v EtOAc:Hexanes) to give the product as an off-white solid in 77% yield (0.3103 g, 1.26 mmol). ^{1}H NMR (500 MHz, CDCl₃) δ 9.58 (s, 1H), 4.62 (d, J = 90.0 Hz, 1H), 3.15 (d, J = 19.2 Hz, 2H), 2.11−1.66 (m, 6H), 1.47 (d, J = 42.9 Hz, 9H). ^{13}C NMR (126 MHz, CDCl₃) δ 200.54, 200.26, 153.47, 151.73, 81.60, 81.30, 71.89, 71.59, 70.75, 70.14, 30.36, 29.37, 29.18, 28.46, 28.36, 28.33, 27.66.

(S)-2-(4-(Dimethoxymethyl)-4,5-dihydrothiazol-2-yl)-N,N-diethylbenzo[d]thiazol-6-amine (9, AlDeLuc). To a round-bottom flask containing **8** (200 mg, 0.82 mmol, 1.0 equiv) dissolved in degassed MeOH (1.63 mL, 0.5 M), was added 4 M hydrochloric acid in dioxanes (2.04 mL, 8.15 mmol, 10.0 equiv). The resulting solution was stirred at room temperature under nitrogen for 16 h. The following day, the solvent was removed by vigorously bubbling nitrogen into the reaction. The resultant oil was then treated with tris(2-carboxyethyl)phosphine hydrochloride (TCEP•HCl) (0.3973 g, 1.39 mmol, 1.70 equiv) dissolved in degassed deionized water (1.33 mL, 1.04 M). After 10 min, the mixture was basified with degassed saturated Cs₂CO₃ in DMF. Compound **4** (0.2074 g, 0.90 mmol, 1.10 equiv) was suspended in degassed tetrahydrofuran (1.34 mL, 0.67 M) and immediately added to the reaction vessel and heated to 50 °C for 1.5 days. The reaction was cooled to room temperature, diluted with water, and extracted with EtOAc (×3). The organic fraction was washed with brine (×1), dried with Na₂SO₄, and concentrated. The crude oil was purified by silica gel column chromatography (eluent: 2:8 v/v EtOAc:Hexanes) to afford a dark orange oil in 66% yield (0.2118 g, 0.54 mmol). ^{1}H NMR (500 MHz, CDCl₃) δ 7.91 (d, J = 9.3 Hz, 1H), 6.98 (d, J = 2.6 Hz, 1H), 6.91 (dd, J = 9.3, 2.6 Hz, 1H), 4.87 (td, J = 8.9, 5.1 Hz, 1H), 4.63 (d, J = 5.1 Hz, 1H), 3.57−3.38 (m, 12H), 1.22 (t, J = 7.1 Hz, 6H). ^{13}C NMR (500 MHz, CDCl₃) δ 164.97, 155.02, 147.29, 144.53, 139.07, 124.94, 113.18, 105.56, 105.52, 101.08, 80.10, 56.05, 55.50, 48.88, 33.01, 12.61. HRMS [M + H]⁺ calculated mass for C₁₇H₂₃N₃O₂S₂ = 366.1305, found = 366.1310

(S)-2-(4-(Diethoxymethyl)-4,5-dihydrothiazol-2-yl)-N,N-diethylbenzo[d]thiazol-6-amine (10). To a round-bottom flask containing **8** (200 mg, 0.82 mmol, 1.0 equiv) dissolved in degassed EtOH (1.63 mL, 0.5 M), was added 4 M hydrochloric acid in dioxanes (2.04 mL, 8.15 mmol, 10.0 equiv) and stirred at room temperature under nitrogen for 16 h. The following day, the solvent was removed by vigorously bubbling nitrogen into the reaction. The resultant oil was then treated with tris(2-carboxyethyl)phosphine hydrochloride (TCEP•HCl) (0.3973 g, 1.39 mmol, 1.70 equiv) dissolved in degassed deionized water (1.33 mL, 1.04 M). After 10 min, the mixture was basified with degassed saturated Cs₂CO₃ in DMF. Compound **4** (0.2074 g, 0.90 mmol, 1.10 equiv) was suspended in degassed tetrahydrofuran (1.34 mL, 0.67 M) and immediately added to the reaction vessel and heated to 50 °C for 1.5 days. The reaction was cooled to room temperature, diluted with

water, and extracted with EtOAc (×3). The organic fraction was washed with brine (×1), dried with Na₂SO₄, and concentrated. The crude oil was purified by silica gel column chromatography (eluent: 2:8 v/v EtOAc:Hexanes) to afford a dark orange oil in 91% yield (0.2920 g, 0.75 mmol). ^{1}H NMR (500 MHz, CDCl₃) δ 7.91 (d, J = 9.2 Hz, 1H), 6.98 (d, J = 2.6 Hz, 1H), 6.91 (dd, J = 9.2, 2.6 Hz, 1H), 4.87 (ddd, J = 9.2, 8.2, 4.6 Hz, 1H), 4.79 (d, J = 4.7 Hz, 1H), 3.85−3.73 (m, 2H), 3.73−3.53 (m, 3H), 3.50−3.38 (m, 5H), 1.28 (t, J = 7.1 Hz, 3H), 1.20 (dt, J = 18.4, 7.0 Hz, 9H). ^{13}C NMR (500 MHz, CDCl₃) δ 164.73, 155.20, 147.27, 144.56, 139.03, 124.94, 113.15, 103.24, 101.09, 80.79, 64.51, 63.60, 44.88, 32.98, 15.44, 15.33, 12.61. HRMS [M + H]⁺ calculated mass for C₁₉H₂₈N₃O₂S₂ = 394.1617, found = 394.1623.

(S)-2-(4-(Diisopropoxymethyl)-4,5-dihydrothiazol-2-yl)-N,N-diethylbenzo[d]thiazol-6-amine (11). To a round-bottom flask containing **8** (200 mg, 0.82 mmol, 1.0 equiv) dissolved in degassed iPrOH (1.63 mL, 0.5 M), was added 4 M hydrochloric acid in dioxanes (2.04 mL, 8.15 mmol, 10.0 equiv) and stirred at room temperature under nitrogen for 16 h. The following day, the solvent was removed by vigorously bubbling nitrogen into the reaction. The resultant oil was then treated with tris(2-carboxyethyl)phosphine hydrochloride (TCEP•HCl) (0.3973 g, 1.39 mmol, 1.70 equiv) dissolved in degassed deionized water (1.33 mL, 1.04 M). After 10 min, the mixture was basified with degassed saturated Cs₂CO₃ in DMF. Compound **4** (0.2074 g, 0.90 mmol, 1.10 equiv) was suspended in degassed tetrahydrofuran (1.34 mL, 0.67 M) and was immediately added to the reaction vessel and heated to 50 °C for 1.5 days. The reaction was cooled to room temperature, diluted with water, and extracted with EtOAc (×3). The organic fraction was washed with brine (×1), dried with Na₂SO₄, and concentrated. The crude oil was purified by silica gel column chromatography (eluent: 5:95 v/v EtOAc:Hexanes) to afford a dark orange oil in 42% yield (0.1444 g, 0.34 mmol). ^{1}H NMR (500 MHz, CDCl₃) δ 7.92 (d, J = 9.1 Hz, 1H), 6.99 (d, J = 2.5 Hz, 1H), 6.91 (dd, J = 9.2, 2.5 Hz, 1H), 4.97 (d, J = 4.0 Hz, 1H), 4.83 (td, J = 8.8, 4.0 Hz, 1H), 3.94 (m, 6.2 Hz, 2H), 3.61 (dd, J = 11.0, 8.2 Hz, 1H), 3.43 (q, J = 7.1 Hz, 5H), 1.27−1.18 (m, 15H), 1.08 (d, J = 6.1 Hz, 3H). ^{13}C NMR (500 MHz, CDCl₃) δ 164.48, 155.33, 147.25, 144.60, 138.98, 124.95, 113.12, 101.11, 99.60, 81.67, 70.18, 68.95, 44.88, 32.71, 23.20, 23.09, 22.59, 22.27, 12.61. HRMS [M + H]⁺ calculated mass for C₂₁H₃₂N₃O₂S₂ = 422.1930, found = 422.1939.

AlDeLuc Isoform Selectivity Assay

Activation of AlDeLuc was assessed using the necessary amount of enzyme that gave the activity of 0.5 nmol of substrate turned over/min. All enzymatic reactions were performed in 50 mM triethanolamine (TEA) buffer (pH 7.4) with 2.5 mM NAD+. To prepare the probe solution, AlDeLuc was dissolved in DMSO and incubated with 1 M HCl. After an hour, this solution was neutralized with 1 M NaOH, and diluted with PBS. To a clear 24-well plate, TEA buffer, NAD+, the ALDH isoform, and then AlDeLuc (2 μM) were added sequentially to a final volume of 1 mL. After an hour incubation at room temperature, ATP-MgSO₄ (45 μL, prepared by mixing 17.78 mM ATP-Mg and 35.56 mM MgSO₄ in a 1:1 ratio in PBS buffer) and luciferase (5 μL, 1 mg/mL in PBS containing 10% glycerol) were added to initiate bioluminescence production. The wells were immediately imaged using the IVIS imaging system in open mode. ROIs were drawn around each well and the signal intensity was quantified using the Living Image Analysis. The signal enhancement was normalized relative to the ALDH2 isoform.

Validation of AlDeLuc Stability in Primary Bone Marrow CD34+ Cells

100 μL of media from each flask was removed and then incubated with the AlDeLuc such that the final concentration of the probe was 20 μM and 0.1% DMSO. After 60 min this solution was aspirated, washed with fresh PBS, and detached from the culture flasks. The cells were then transferred to a 15 mL centrifuge tube and pelleted at 1000 rpm for 5 min at room temp. The cells were resuspended in PBS along with 10% protease inhibitor solution (1 protease inhibitor mini tablet per 10 mL of PBS, Pierce, Thermo Fisher Scientific) and

sonicated on ice for 2.5 min (pulse 01, 01, 40%). The cell debris was removed via centrifugation, the supernatant was plated (95 μL/well) into a 96-well plate (n = 5 for each condition), and treated with luciferase (5 μL, 1 mg/mL) and immediately imaged using the IVIS imaging system in open mode. ROIs were drawn around each well and the signal intensity was quantified using the Living Image Analysis software. All data reported as the mean $\pm$ standard deviation (n = 5).

Confirmation of ALDH1A1-Mediated Activation of AlDeLuc in Human Lung Cancer Cells Using NCT-501•HCl

A549 cells were cultured in T75 culture flasks. Once cells had become ~90% confluent, the media was replaced with fresh F-12K media (8.920 mL). AlDeLuc was dissolved in a DMSO and diluted to 200 μM with HAMS F-12K media (1% v/v final DMSO). Either ALDH1A1-specific inhibitor, NCT-501•HCl, (5 mM in PBS, final concentration 40 μM) or a vehicle was added to the culture flask. Immediately after, 1 mL of the AlDeLuc solution was added to each flask (final concentration 20 μM, 0.1% v/v final DMSO concentration). After incubation for one hour, the solutions were aspirated, the cells were washed with PBS (×2) and detached from the culture flasks. The cells were then transferred to a 15 mL centrifuge tube and pelleted at 1000 rpm for 5 min at room temp. The cells were resuspended in PBS along with 10% protease inhibitor solution (1 protease inhibitor mini tablet per 10 mL of PBS, Pierce, Thermo Fisher Scientific) and sonicated on ice for 2.5 min (pulse 01, 01, 40%). The cell debris was removed via centrifugation, the supernatant was plated (95 μL/well) into a 96-well plate (n = 5 for each condition), and treated with luciferase (5 μL, 1 mg/mL) and immediately imaged using the IVIS imaging system in open mode. ROIs were drawn around each well and the signal intensity was quantified using the Living Image Analysis software. All data reported as the mean $\pm$ standard deviation (n = 4).

Generation of Orthotopic 4T1-Luc Tumors for Diet Study

Female BALB/c mice (~6 weeks old) were placed on a high-fat diet (Research Diets no. D12492) where 60% of calories are from fat. After a 20-week priming period, animals were inoculated with 4T1-Luc cells (50 μL of 1×10^5 cells in 1:1 v/v serum-free RPMI 1640 media and Matrigel) via subcutaneous injections into the mammary fat pad. That same day the mice were randomly divided into two groups in which the control group received water, while the experimental group was administered L-NMMA (50 mg/kg) via oral gavage. Oral gavage treatment continued daily for 20 days. Tumor volumes were measured using the caliper method every 3 days. Body weight was measured daily over the course of the experiment.

Bioluminescence Imaging of High-Fat Diet Breast Cancer Model with AlDeLuc

The day following final L-NMMA oral gavage treatment both groups of mice were anesthetized using isoflurane (1−3% for maintenance; up to 5% for induction) in oxygen from a precision vaporizer. After testing to ensure animals are fully under anesthesia, each mouse was administered a solution of AlDeLuc (0.55 mg/kg, 1:19 v/v DMSO:PBS). After 40 min, the mice were imaged on the IVIS imaging system. Luminescence was collected using an open filter set. ROIs were drawn around the mammary fat-pad tumor and the intensity was calculated using the Living Image Analysis software.

■ ASSOCIATED CONTENT

ⓢ Supporting Information

The Supporting Information is available free of charge at https://pubs.acs.org/doi/10.1021/jacsau.4c01001.

> Further experimental details, including synthetic procedures, spectral characterizations, and supplemental in vitro and in vivo procedures and data (PDF)

■ AUTHOR INFORMATION

Corresponding Author

Jefferson Chan − *Department of Chemistry, Beckman Institute for Advanced Science and Technology, and Cancer Center at Illinois, University of Illinois Urbana−Champaign, Urbana, Illinois 61801, United States;* ⓘ orcid.org/0000-0003-4139-4379; Email: jeffchan@illinois.edu

Authors

Chelsea B. Swartchick − *Department of Chemistry, Beckman Institute for Advanced Science and Technology, and Cancer Center at Illinois, University of Illinois Urbana−Champaign, Urbana, Illinois 61801, United States*

Musa Dirak − *Department of Chemistry, Beckman Institute for Advanced Science and Technology, and Cancer Center at Illinois, University of Illinois Urbana−Champaign, Urbana, Illinois 61801, United States;* ⓘ orcid.org/0000-0002-2085-2345

Lily C. F. Wenger − *Department of Chemistry, Beckman Institute for Advanced Science and Technology, and Cancer Center at Illinois, University of Illinois Urbana−Champaign, Urbana, Illinois 61801, United States*

Rodrigo Tapia Hernandez − *Department of Chemistry, Beckman Institute for Advanced Science and Technology, and Cancer Center at Illinois, University of Illinois Urbana−Champaign, Urbana, Illinois 61801, United States;* ⓘ orcid.org/0000-0002-0462-7711

Michael C. Lee − *Department of Chemistry, Beckman Institute for Advanced Science and Technology, and Cancer Center at Illinois, University of Illinois Urbana−Champaign, Urbana, Illinois 61801, United States;* ⓘ orcid.org/0000-0001-8125-7120

Complete contact information is available at:
https://pubs.acs.org/10.1021/jacsau.4c01001

Author Contributions

C.B.S. synthesized AlDeLuc and its derivatives, performed in vitro characterizations, selectivity studies, in cellulo experiments, generated the allograft breast cancer models, and performed BL imaging with assistance from L.C.F.W., M.D. assisted with in vitro, cellular, and BL imaging experiments. L.C.F.W. and C.B.S. performed oral gavage administration and monitored mice tumor volumes and weights. R.T.H. and C.B.S. performed organ excision and validated b-galactosidase enzyme activity. C.B.S. and M.C.L. expressed purified all ALDH isoforms. All authors analyzed and interpreted the data. C.B.S. and J.C. wrote the manuscript. All authors have given approval to the final version of the manuscript.

■ ACKNOWLEDGMENTS

■ ABBREVIATIONS

CSCs	cancer stem cells
ALDH1A1	aldehyde dehydrogenase 1A1
TME	tumor microenvironment
DETA NONOate	(Z)-1-[N-(2-aminoethyl)-N-(2-ammonioethyl)amino]diazen-1-ium-1,2-diolate
L-NMMA	L-NG-monomethyl arginine acetate
HPLC-MS	high performance liquid chromatography−mass spectrometry
NO	nitric oxide
IFN-γ	interferon-gamma
PBS	phosphate buffered saline
ROI	region of interest

■ REFERENCES

(1) Khoury, T.; Ademuyiwa, F. O.; Chandrasekhar, R.; Jabbour, M.; DeLeo, A.; Ferrone, S.; Wang, Y.; Wang, X. Aldehyde dehydrogenase 1A1 expression in breast cancer is associated with stage, triple negativity, and outcome to neoadjuvant chemotherapy. *Modern Pathol.* 2012, 25 (3), 388−397.

(2) Tomita, H.; Tanaka, K.; Tanaka, T.; Hara1, A. Aldehyde dehydrogenase 1A1 in stem cells and cancer. *Oncotarget* 2016, 7 (10), 11018−11032.

(3) Vasiliou, V.; Pappa, A.; Petersen, D. R. Role of aldehyde dehydrogenases in endogenous and xenobiotic metabolism. *Chem.-Biol. Interact* 2000, 129 (1−2), 1−19.

(4) Vassalli, G. Aldehyde Dehydrogenases: Not Just Markers, but Functional Regulators of Stem Cells. *Stem Cells Int.* 2019, 2019, 1−15.

(5) Yue, H.; Hu, Z.; Hu, R.; Guo, Z.; Zheng, Y.; Wang, Y.; Zhou, Y. ALDH1A1 in Cancers: Bidirectional Function, Drug Resistance, and Regulatory Mechanism. *Front. Oncol.* 2022, 12, 1−11.

(6) Datta, N.; Snijesh, S.; Parvathy, K.; Sneha, A. S.; Maliekal, T. T. ALDH1A1 as a marker for metastasis initiating cells: A mechanistic insight. *Exp. Cell Res.* 2024, 442 (1), 114213.

(7) Storms, R. W.; Trujillo, A. P.; Springer, J. B.; Shah, L.; Colvin, O. M.; Ludeman, S. M.; Smith, C. Isolation of primitive human hematopoietic progenitors on the basis of aldehyde dehydrogenase activity. *Proc. Natl. Acad. Sci. U. S. A.* 1999, 96, 9118−9123.

(8) Duan, J. J.; Cai, J.; Gao, L.; Yu, S. C. ALDEFLUOR activity, ALDH isoforms, and their clinical significance in cancers. *J. Enzyme Inhib. Med. Chem.* 2023, 38 (1), 2166035.

(9) Zhou, L.; Sheng, D.; Wang, D.; Ma, W.; Deng, Q.; Deng, L.; Liu, S. Identification of cancer-type specific expression patterns for active aldehyde dehydrogenase (ALDH) isoforms in ALDEFLUOR assay. *Cell Bio. Toxicol.* 2019, 35 (2), 161−177.

(10) Bearrood, T. E.; Aguirre-Figueroa, G.; Chan, J. Rational Design of a Red Fluorescent Sensor for ALDH1A1 Displaying Enhanced Cellular Uptake and Reactivity. *Bioconjugate Chem.* 2020, 31 (2), 224−228.

(11) Anorma, C.; Hedhli, J.; Bearrood, T. E.; Pino, N. W.; Gardner, S. H.; Inaba, H.; Zhang, P.; Li, Y.; Feng, D.; Dibrell, S. E. Surveillance of Cancer Stem Cell Plasticity Using an Isoform-Selective Fluorescent Probe for Aldehyde Dehydrogenase 1A1. *ACS Cent. Sci.* 2018, 4 (8), 1045−1055.

(12) Yadav, A. K.; Chan, J. Activity-based bioluminescence probes for in vivo sensing applications. *Curr. Opin. Chem. Biol.* 2023, 74, 102310.

(13) Xia, T.; Cheng, X.; Zhan, W.; Liang, G. Activity-Based Luciferase-Luciferin Bioluminescence System for Bioimaging Applications. *Anal. Sens.* 2021, 1 (4), 138−147.

(14) Kojima, R.; Takakura, H.; Kamiya, M.; Kobayashi, E.; Komatsu, T.; Ueno, T.; Terai, T.; Hanaoka, K.; Nagano, T.; Urano, Y. Development of a Sensitive Bioluminogenic Probe for Imaging Highly Reactive Oxygen Species in Living Rats. *Angew. Chem., Int. Ed.* 2015, 54 (49), 14768−14771.

(15) Bruemmer, K. J.; Crossley, S. W. M.; Chang, C. J. Activity-Based Sensing: A Synthetic Methods Approach for Selective Molecular Imaging and Beyond. *Angew. Chem., Int. Ed.* 2020, 59 (33), 13734−13762.

(16) Li, J. B.; Chen, L.; Wang, Q.; Liu, H. W.; Hu, X. X.; Yuan, L.; Zhang, X. B. A Bioluminescent Probe for Imaging Endogenous Peroxynitrite in Living Cells and Mice. *Anal. Chem.* 2018, 90 (6), 4167−4173.

(17) Heffern, M. C.; Park, H. M.; Au-Yeung, H. Y.; Van de Bittner, G. C.; Ackerman, C. M.; Stahl, A.; Chang, C. J. In vivo bioluminescence imaging reveals copper deficiency in a murine model of nonalcoholic fatty liver disease. *Proc. Natl. Acad. Sci. U. S. A.* 2016, 113 (50), 14219−14224.

(18) Van de Bittner, G. C.; Dubikovskaya, E. A.; Bertozzi, C. R.; Chang, C. J. In vivo imaging of hydrogen peroxide production in a murine tumor model with a chemoselective bioluminescent reporter. *Proc. Natl. Acad. Sci. U. S. A.* 2010, 107 (50), 21316−21321.

(19) Liu, X.; Tian, X.; Xu, X.; Lu, J. Design of a phosphinate-based bioluminescent probe for superoxide radical anion imaging in living cells. *Luminescence* 2018, 33 (6), 1101−1106.

(20) Aron, A. T.; Heffern, M. C.; Lonergan, Z. R.; Vander Wal, M. N.; Blank, B. R.; Spangler, B.; Zhang, Y.; Park, H. M.; Stahl, A.; Renslo, A. R. In vivo bioluminescence imaging of labile iron accumulation in a murine model of Acinetobacter baumannii infection. *Proc. Natl. Acad. Sci. U. S. A.* 2017, 114 (48), 12669−12674.

(21) Van de Bittner, G. C.; Bertozzi, C. R.; Chang, C. J. Strategy for dual-analyte luciferin imaging: in vivo bioluminescence detection of hydrogen peroxide and caspase activity in a murine model of acute inflammation. *J. Am. Chem. Soc.* 2013, 135 (5), 1783−1795.

(22) Yadav, A. K.; Lee, M. C.; Lucero, M. Y.; Su, S.; Reinhardt, C. J.; Chan, J. Activity-Based NIR Bioluminescence Probe Enables Discovery of Diet-Induced Modulation of the Tumor Microenvironment via Nitric Oxide. *ACS Cent. Sci.* 2022, 8 (4), 461−472.

(23) Wang, B.; Chen, X.; Wang, Z.; Xiong, W.; Xu, T.; Zhao, X.; Cao, Y.; Guo, Y.; Lin, L.; Chen, S. Aldehyde dehydrogenase 1A1 increases NADH levels and promotes tumor growth via glutathione/dihydrolipoic acid-dependent NAD+ reduction. *Oncotarget* 2017, 8 (40), 67043−67055.

(24) Ma, I.; Allan, A. L. The Role of Human Aldehyde Dehydrogenase in Normal and Cancer Stem Cells. *Stem Cell Rev. Rep.* **2011**, *7* (2), 292–306.

(25) Boedtkjer, E.; Pedersen, S. F. The Acidic Tumor Microenvironment as a Driver of Cancer. *Annu. Rev. Physiol.* **2020**, *82*, 103–126.

(26) Ko, M.; Quinones-Hinojosa, A.; Rao, R. Emerging links between endosomal pH and cancer. *Cancer Metastasis Rev.* **2020**, *39* (2), 519–534.

(27) Yadav, A. K.; Reinhardt, C. J.; Arango, A. S.; Huff, H. C.; Dong, L.; Malkowski, M. G.; Das, A.; Tajkhorshid, E.; Chan, J. An Activity-Based Sensing Approach for the Detection of Cyclooxygenase-2 in Live Cells. *Angew. Chem., Int. Ed.* **2020**, *59* (8), 3307–3314.

(28) Lucero, M. Y.; Gardner, S. H.; Yadav, A. K.; Borri, A.; Zhao, Z.; Chan, J. Activity-based Photoacoustic Probes Reveal Elevated Intestinal MGL and FAAH Activity in a Murine Model of Obesity. *Angew. Chem., Int. Ed.* **2022**, *61* (44), No. e202211774.

(29) Gardner, S. H.; Reinhardt, C. J.; Chan, J. Advances in Activity-Based Sensing Probes for Isoform-Selective Imaging of Enzymatic Activity. *Angew. Chem., Int. Ed.* **2021**, *60* (10), 5000–5009.

(30) Nakatsu, T.; Ichiyama, S.; Hiratake, J.; Saldanha, A.; Kobashi, N.; Sakata, K.; Kato, H. Structural basis for the spectral difference in luciferase bioluminescence. *Nature* **2006**, *440* (7082), 372–376.

(31) Liang, Z.; Koivikko, H.; Oivanen, M.; Heinonen, P. Tuning the stability of alkoxyisopropyl protection groups. *Beilstein J. Org. Chem.* **2019**, *15*, 746–751.

(32) Meisenheimer, P. L.; Uyeda, H. T.; Ma, D.; Sobol, M.; McDougall, M. G.; Corona, C.; Simpson, D.; Klaubert, D. H.; Cali, J. J. Proluciferin acetals as bioluminogenic substrates for cytochrome P450 activity and probes for CYP3A inhibition. *Drug Metab. Dispos.* **2011**, *39* (12), 2403–2410.

(33) Wei, Y.; Li, Y.; Chen, Y.; Liu, P.; Huang, S.; Zhang, Y.; Sun, Y.; Wu, Z.; Hu, M.; Wu, Q. ALDH1: A potential therapeutic target for cancer stem cells in solid tumors. *Front. Oncol.* **2022**, *12*, 1026278.

(34) Huang, T.-C.; Chen, M.-H.; Ho, C.-T. Effect of Phosphate on Stability of Pyridoxal in the Presence ofLysine. *J. Agric. Food Chem.* **2001**, *49* (3), 1559–1563.

(35) Zhang, L.; Tam, J. P. Thiazolidine Formation as a General and Site-Specific Conjugation Method for Synthetic Peptides and Proteins. *Anal. Biochem.* **1996**, *233*, 87–93.

(36) Agarwal, P.; van der Weijden, J.; Sletten, E. M.; Rabuka, D.; Bertozzi, C. R. A Pictet-Spengler ligation for protein chemical modification. *Proc. Natl. Acad. Sci. U. S. A.* **2013**, *110* (1), 46–51.

(37) Muramoto, G. G.; Russell, J. L.; Safi, R.; Salter, A. B.; Himburg, H. A.; Daher, P.; Meadows, S. K.; Doan, P.; Storms, R. W.; Chao, N. J. Inhibition of Aldehyde Dehydrogenase Expands Hematopoietic Stem Cells with Radioprotective Capacity. *Stem Cells* **2010**, *28* (3), 523–534.

(38) Storms, R. W.; Green, P. D.; Safford, K. M.; Niedzwiecki, D.; Cogle, C. R.; Colvin, O. M.; Chao, N. J.; Rice, H. E.; Smith, C. A. Distinct hematopoietic progenitor compartments are delineated by the expression of aldehyde dehydrogenase and CD34. *Blood* **2005**, *106* (1), 95–102.

(39) Stouras, I.; Vasileiou, M.; Kanatas, P. F.; Tziona, E.; Tsianava, C.; Theocharis, S. Metabolic Profiles of Cancer Stem Cells and Normal Stem Cells and Their Therapeutic Significance. *Cells* **2023**, *12* (23), 2686.

(40) Liu, Y.; White, K. A.; Barber, D. L. Intracellular pH Regulates Cancer and Stem Cell Behaviors: A Protein Dynamics Perspective. *Front. Oncol.* **2020**, *10*, 1–7.

(41) Rodimova, S. A.; Meleshina, A. V.; Kalabusheva, E. P.; Dashinimaev, E. B.; Reunov, D. G.; Torgomyan, H. G.; Vorotelyak, E. A.; Zagaynova, E. V. Metabolic activity and intracellular pH in induced pluripotent stem cells differentiating in dermal and epidermal directions. *Methods Appl. Fluoresc.* **2019**, *7* (4), 044002.

(42) Park, J. W.; Jung, K. H.; Lee, J. H.; Moon, S. H.; Cho, Y. S.; Lee, K. H. Inhibition of aldehyde dehydrogenase 1 enhances the cytotoxic effect of retinaldehyde on A549 cancer cells. *Oncotarget* **2017**, *8* (59), 99382–99393.

(43) Li, Z.; Xiang, Y.; Xiang, L.; Xiao, Y.; Li, F.; Hao, P. ALDH maintains the stemness of lung adenoma stem cells by suppressing the Notch/CDK2/CCNE pathway. *PLoS One* **2014**, *9* (3), No. e92669.

(44) Yang, S. M.; Yasgar, A.; Miller, B.; Lal-Nag, M.; Brimacombe, K.; Hu, X.; Sun, H.; Wang, A.; Xu, X.; Nguyen, K. Discovery of NCT-501, a Potent and Selective Theophylline-Based Inhibitor of Aldehyde Dehydrogenase 1A1 (ALDH1A1). *J. Med. Chem.* **2015**, *58* (15), 5967–5978.

(45) Moon, K.-H.; Abdelmegeed, M. A.; Song, B.-J. Inactivation of cytosolic aldehyde dehydrogenase via S-nitrosylation in ethanol-exposed rat liver. *FEBS Lett.* **2007**, *581* (21), 3967–3972.

(46) Kim, R. J.; Park, J. R.; Roh, K. J.; Choi, A. R.; Kim, S. R.; Kim, P. H.; Yu, J. H.; Lee, J. W.; Ahn, S. H.; Gong, G. High aldehyde dehydrogenase activity enhances stem cell features in breast cancer cells by activating hypoxia-inducible factor-2α. *Cancer Lett.* **2013**, *333* (1), 18–31.

(47) Zhuang, X.; Shi, G.; Hu, X.; Wang, H.; Sun, W.; Wu, Y. Interferon-gamma inhibits aldehyde dehydrogenasebright cancer stem cells in the 4T1 mouse model of breast cancer. *Chin. Med. J.* **2022**, *135* (2), 194–204.

(48) Su, Y.; Qiu, Q.; Zhang, X.; Jiang, Z.; Leng, Q.; Liu, Z.; Stass, S. A.; Jiang, F. Aldehyde Dehydrogenase 1 A1−Positive Cell Population Is Enriched in Tumor-Initiating Cells and Associated with Progression of Bladder Cancer. *Cancer Epidemio. Biomarkers Prevent* **2010**, *19* (2), 327–337.

(49) Ma, K.; Yue, Y.; Zhao, L.; Chao, J.; Yin, C. A sequentially activated bioluminescent probe for observation of cellular H2O2 production induced by cysteine. *Chem. Commun.* **2021**, *57* (78), 10015–10018.

(50) Cheng, X.; Xia, T.; Sun, X.; Liang, G.; Liu, X.; Liang, G. Atg4B and Cathepsin B-Triggered in Situ Luciferin Formation for Precise Cancer Autophagy Bioluminescence Imaging. *ACS Cent. Sci.* **2023**, *9* (12), 2251–2256.

(51) Henkin, A. H.; Cohen, A. S.; Dubikovskaya, E. A.; Park, H. M.; Nikitin, G. F.; Auzias, M. G.; Kazantzis, M.; Bertozzi, C. R.; Stahl, A. Real-time noninvasive imaging of fatty acid uptake in vivo. *ACS Chem. Biol.* **2012**, *7* (11), 1884–1891.

(52) Duellman, S. J.; Valley, M. P.; Kotraiah, V.; Vidugiriene, J.; Zhou, W.; Bernad, L.; Osterman, J.; Kimball, J. J.; Meisenheimer, P.; Cali, J. J. A bioluminescence assay for aldehyde dehydrogenase activity. *Anal. Biochem.* **2013**, *434* (2), 226–232.

(53) Liu, L.; Mei, M.; Yang, S.; Li, Q. Roles of chronic low-grade inflammation in the development of ectopic fat deposition. *Mediators Inflamm.* **2014**, *2014*, 418185.